Ferromagnetic proximity effect in a ferromagnet/iron-pnictide superconductor junction

A Letters Journal Exploring the Frontiers of Physics

October 2011

EPL, **96** (2011) 17009
doi: 10.1209/0295-5075/96/17009

www.epljournal.org

Ferromagnetic proximity effect in a ferromagnet/iron-pnictide superconductor junction

Y. C. Tao[1(a)] and J. G. Hu[2]

[1] *Department of Physics, Nanjing Normal University - Nanjing 210097, China*
[2] *Department of Physics, Yangzhou University - Yangzhou 225002, China*

received 21 June 2011; accepted in final form 17 August 2011
published online 21 September 2011

PACS 74.45.+c – Proximity effects; Andreev reflection; SN and SNS junctions
PACS 74.50.+r – Tunneling phenomena; Josephson effects
PACS 74.20.Rp – Pairing symmetries (other than *s*-wave)

Abstract – The proximity effect in a bilayer consisting of a ferromagnet (FM) and an iron-pnictide superconductor (SC) with antiphase *s*-wave pairing is first studied by extending Nambu spinor Green's function approach. Due to the opposite signs of the two pair potentials in the SC, the order parameters in the FM and SC regions at the interface induced by the proximity effect are not only noncontinuous but also antiphase and the barrier strength has a significant influence on the peak and dip behaviors of the induced superconducting density of states (DOS) in the two regions. Particularly, one conspicuously characteristic peak of the DOS at either gap energy in the SC appears. These properties are much different from those without antiphase *s*-wave pairing for the SC, which can be applied to experimentally identify the antiphase *s*-wave pairing in iron-based SCs.

Introduction. – Very recently, multiband superconductivity has again attracted much attention, particularly after the discovery of high-temperature superconductivity in the family of intrinsically multiband iron-based materials [1–12]. As faced by all newly discovered superconductors (SCs) with unconventional behaviors, one of the important issues for the iron-based SCs are their pairing symmetries. Though much effort has been devoted to this issue, the controversy remains [7], such many order parameter (OP) symmetries as *s*-wave and *d*-wave were put forward. A leading contender is the so-called antiphase *s*-wave or $s_{\pm}$-pairing of multiband SC, in which the pair potentials for the hole and electron bands are of the isotropic *s*-wave state but they have opposite signs. It is important to confirm the $s_{\pm}$-paring in the iron-based SCs by experiments.

On the other hand, the proximity effect in ferromagnet (FM)/SC has been of long-standing research interest and recently also attracted much attention [13–16]. The proximity effect has two implications. One is the mutual leakage of magnetic and superconducting properties near the FM/SC interface, such as rapidly damped oscillation of singlet superconductivity on the FM side and spin-depedent gapless superconductivity on the SC side [14–16]. And the other is that the competition between two types of mutually exclusive long-range orderings leads to a rich variety of phenomena, for example, the appearance of spin-triplet pairing states [13]. Andreev reflection (AR) plays an important role in the SC/FM proximity effect [17,18]. An electron-like quasiparticle in FM with energy lower than the superconducting energy gap cannot enter into the SC and performs via AR. It is reflected at the FM/SC interface as a hole. The constructive interference of electron-like and hole-like quasiparticles causes Andreev bound states in FM, which has a great impact on the transfer of the polarized electron-like particles through the junction. However, due to the spin splitting of the energy band, the spin of the quasiparticle may be reversed, and this means that the exchange energy is gained or lost by a quasiparticle Andreev-reflected at the interface. Probing the proximity effect, such as the density of states (DOS) in the FM and SC, has proven itself as a highly useful tool to access information about the symmetry of superconducting OP [19–23]. So far, however, there has been no reports on the ferromagnetic proximity effect in an FM/iron-based SC junction. It is expected that the study of the proximity effect will uncover some novel properties and provide a powerful tool for probing and identifying the $s_{\pm}$-pairing in iron-based SCs.

In this work, by taking into account the interband interference between the two bands in the iron-based SC as also in other multiband systems, we first extend the

(a) E-mail: isyctao88@163.com

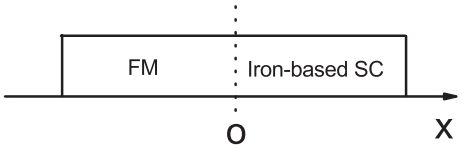

Fig. 1: Schematic illustration of the FM/iron-based SC bilayer.

Nambu spinor Green's function approach to studying the ferromagnetic proximity in an FM/iron-based SC junction with a ballistic Andreev contact. It is found that the OPs in the FM and SC regions near the FM/SC interface induced by the proximity effect are not only uncontinuous but also antiphase. The peak and dip behaviors of the induced superconducting DOS in the FM and SC are determined by both the barrier strength and the mixing coefficient of the two bands in the iron-based SC. More importantly, there exists one conspicuously characteristic peak of the induced superconducting DOS at either energy on the SC side. These properties are much different from those for the SC without antiphase s-wave or with s_{++}-pairing, which could be helpful in determining the paring symmetry. The work is organized as follows. In the second section, we give the model and theory. In the third section, we make numerical calculations and give the discussions. Finally, the summary is given in the last section.

Model and theory. – We consider a ballistic Andreev ferromagnetic contact modeled by the x-direction with an FM to the left of $x=0$ and an $s_{\pm}$-pairing SC to the right as shown in fig. 1. The FM/SC interface at $x=0$ is described by a δ-type barrier potential $U(x)=U_0\delta(x)$ with U_0 being dependent on the product of the barrier and width. A subband model with spin-splitting energy Γ is applied for the FM whose exchange energy described by $h(x)=h_0\Theta(-x)$, where $\Theta(x)$ is the Heaviside step function and h_0 is equal to $\Gamma/2$. The iron-based SC has two superconducting gap energies $\Delta_{1,2}$ in both bands with corresponding Fermi wave vectors p and q, and the relevant superconducting phases are $\varphi_{1,2}$. For the $s_{\pm}$-pairing model with unequal s-wave gaps of opposite sign, $\varphi_1-\varphi_2=\pi$, while for the s_{++}-pairing model with the gaps of the same sign, $\varphi_1=\varphi_2$. We begin with the Bogoliubov-de Gennes (BdG) equation for the quasiparticle spectrum [24]. In the absence of spin-flip scattering, the spin-dependent (four-component) BdG equation may be decoupled into two sets of two-component equations: one is for the spin-σ electron-like and spin-$\overline{\sigma}$ hole-like quasiparticle wave functions $(u_\sigma, v_{\overline{\sigma}})$, the other is $(u_{\overline{\sigma}}, v_\sigma)$, where σ is the spin index with $\uparrow$ or $\downarrow$ and $\overline{\sigma}$ is the spin opposite to σ, for instance, the BdG equation for $(u_\sigma, v_{\overline{\sigma}})$ is given by

$$\begin{bmatrix} H_0(x)-h(x) & \Delta(x) \\ \Delta^*(x) & -H_0(x)-h(x) \end{bmatrix} \begin{bmatrix} u_\sigma(x) \\ v_{\overline{\sigma}}(x) \end{bmatrix} = E \begin{bmatrix} u_\sigma(x) \\ v_{\overline{\sigma}}(x) \end{bmatrix}, \tag{1}$$

where $H_0(x)=-\hbar^2\nabla_x^2/2m+V(x)-E_F$ with $V(x)$ the usual static potential, and the dispersions are assumed to be parabolic as in refs. [20,22,23], and E the excitation energy measured relative to Fermi energy E_F can be positive or negative and is taken to be positive as in refs. [20, 22,23]. For the injection of a spin-σ electron from the left FM, there are four possible trajectories: normal reflection (b_σ), Andreev reflection ($a_{\overline{\sigma}}$), and transmission to the right FM as an eletron-like quasiparticle (c_σ) and as a hole-like quasiparticle ($d_{\overline{\sigma}}$). With the general solution of eq. (1), the wave functions in the FM/SC junction are given by

$$\psi_1(x)=[e^{ik_+^\sigma x}+b_{1\sigma}e^{-ik_+^\sigma x}]\begin{pmatrix}1\\0\end{pmatrix}+a_{1\bar{\sigma}}e^{ik_-^{\overline{\sigma}}x}\begin{pmatrix}0\\1\end{pmatrix} \tag{2}$$

for $x\leqslant 0$ and

$$\psi_2(x) = c_{1\sigma}\left[e^{ip_+x}\begin{pmatrix}u_1\\v_1\end{pmatrix}+\alpha_0 e^{iq_+x}\begin{pmatrix}u_2\\v_2\end{pmatrix}\right]+ d_{1\bar{\sigma}}\left[e^{-iq_-x}\begin{pmatrix}v_1\\u_1\end{pmatrix}+\alpha_0 e^{-iq_-x}\begin{pmatrix}v_2\\u_2\end{pmatrix}\right] \tag{3}$$

for $x\geqslant 0$, where $k_{+(-)}^\sigma=\sqrt{2m(E_F+(-)E+\eta_\sigma h_0)}/\hbar$ with $\eta_\sigma=1$ for $\sigma=\uparrow$ and $\eta_\sigma=-1$ for $\sigma=\downarrow$, $p_\pm=\sqrt{2m(E_F\pm\Omega_1)}/\hbar$, $q_\pm=\sqrt{2m(E_F\pm\Omega_2)}/\hbar$ with $\Omega_{1(2)}=\sqrt{E^2-\Delta_{1(2)}^2}$, and the mixing coefficient α_0 is defined to describe the ratio of the probability amplitudes for an electron crossing the interface from the left FM to tunnel into the first and second bands in the SC [23]. In eqs. (2), (3), all the transmission and reflection coefficients are determined by usual matching conditions of the wave functions at $x=0$. The wave functions for the other three types of quasiparticle injection processes can be obtained in a similar way.

After obtaining all the wave functions, we can calculate by a similar way the Nambu spinor Green's functions in the FM/SC structure, the retarded Green's function $G_r^\sigma(x,x,E)$ which is constructed from their linear combination [25]. All the coefficients are determined by the equations $G_r^\sigma(x,x+0_+,E)=G_r^\sigma(x,x-0_+,E)$, $\partial G_r^\sigma(x,x',E)/\partial x|_{x=x'+0_+}-\partial G_r^\sigma(x,x',E)/\partial x|_{x=x'-0_+}=(2m/\hbar^2)\hat{\tau}_3$ with $\hat{\tau}_3$ the Pauli matrix. After carrying out a little tedious calculation, we get the Green's functions as

see eq. (4) *on the next page*

in the FM and

see eq. (5) *on the next page*

in the SC. In these expressions,

$$a_{1\bar{\sigma}}= 2k_+^\sigma\frac{(-v_1\beta_4+u_1\beta_3)e^{-i\varphi_1}+\alpha_0(-v_2\beta_4+u_2\beta_3)e^{-i\varphi_2}}{(\beta_2\beta_3-\beta_1\beta_4)\beta_3}, \tag{6}$$

$$b_{1\sigma}=-1+2k_+^\sigma\frac{(-u_1\beta_4+v_1\beta_3)+\alpha_0(-u_2\beta_4+v_2\beta_3)}{(\beta_2\beta_3-\beta_1\beta_4)\beta_3}, \tag{7}$$

$$G_r^\sigma(x,x,E) = -\frac{im}{\hbar^2 k_+^\sigma} \times \left[a_{1\overline{\sigma}} e^{i(k_{\overline{\sigma}}^- - k_+^\sigma)x} \begin{pmatrix} 0 & 0 \\ 1 & 0 \end{pmatrix} + (1 + b_{1\sigma} e^{-2ik_+^\sigma x}) \begin{pmatrix} 1 & 0 \\ 0 & 0 \end{pmatrix} \right] - \frac{im}{\hbar^2 k_-^{\overline{\sigma}}} \left[(1 + a_{2\overline{\sigma}} e^{2ik_-^{\overline{\sigma}} x}) \begin{pmatrix} 0 & 0 \\ 0 & 1 \end{pmatrix} + b_{2\sigma} e^{i(k_-^{\overline{\sigma}} - k_+^\sigma)x} \begin{pmatrix} 0 & 1 \\ 0 & 0 \end{pmatrix} \right] \tag{4}$$

$$\begin{aligned} G_r^\sigma(x,x,E) = & -a_{3\overline{\sigma}} \frac{imE}{\hbar^2} \left[\frac{e^{i(p_+ - p_-)x}}{p_+ \Omega_P} \begin{pmatrix} u_1 v_1 & u_1^2 \\ v_1^2 & u_1 v_1 \end{pmatrix} + \frac{\alpha_0 e^{i(q_+ - q_-)x}}{q_+ \Omega_q} \begin{pmatrix} u_2 v_2 & u_2^2 \\ v_2^2 & u_2 v_2 \end{pmatrix} \right] \\ & - \frac{imE}{\hbar^2} \left[\frac{1}{p_+ \Omega_P} (1 + b_3^\sigma e^{2ip_+ x}) \begin{pmatrix} u_1^2 & u_1 v_1 \\ u_1 v_1 & v_1^2 \end{pmatrix} + \frac{\alpha_0}{q_+ \Omega_q} (1 + b_3^\sigma e^{2iq_+ x}) \begin{pmatrix} u_2^2 & u_2 v_2 \\ u_2 v_2 & v_2^2 \end{pmatrix} \right] \\ & - a_{4\overline{\sigma}} \frac{imE}{\hbar^2} \left[\frac{e^{i(p_+ - p_-)x}}{p_- \Omega_P} \begin{pmatrix} u_1 v_1 & v_1^2 \\ u_1^2 & u_1 v_1 \end{pmatrix} + \frac{\alpha_0 e^{i(q_+ - q_-)x}}{q_+ \Omega_q} \begin{pmatrix} u_2 v_2 & v_2^2 \\ u_2^2 & u_2 v_2 \end{pmatrix} \right] \\ & - \frac{imE}{\hbar^2} \left[\frac{1}{p_- \Omega_P} (1 + b_4^\sigma e^{2ip_+ x}) \begin{pmatrix} v_1^2 & u_1 v_1 \\ u_1 v_1 & u_1^2 \end{pmatrix} + \frac{\alpha_0}{q_- \Omega_q} (1 + b_4^\sigma e^{2iq_- x}) \begin{pmatrix} v_2^2 & u_2 v_2 \\ u_2 v_2 & u_2^2 \end{pmatrix} \right] \end{aligned} \tag{5}$$

$$a_{2\overline{\sigma}} = 2k_-^{\overline{\sigma}} \frac{(v_1\beta_1 - u_1\beta_2) + \alpha_0(v_2\beta_1 - u_2\beta_2)}{(\beta_2\beta_3 - \beta_1\beta_4)\beta_2}, \tag{8}$$

$$b_{2\sigma} = 2k_-^{\overline{\sigma}} \frac{(u_1\beta_1 - v_1\beta_2)e^{-i\varphi_1} + \alpha_0(u_2\beta_1 - v_2\beta_2)e^{-i\varphi_2}}{(\beta_2\beta_3 - \beta_1\beta_4)\beta_2}, \tag{9}$$

$$a_{3\overline{\sigma}} = \frac{-\gamma_2\beta_1 - \gamma_1\beta_3}{-\beta_2\beta_3 + \beta_1\beta_4}, \tag{10}$$

$$b_{3\sigma} = \frac{-\gamma_2\beta_2 - \gamma_1\beta_4}{-\beta_2\beta_3 + \beta_1\beta_4}, \tag{11}$$

$$a_{4\overline{\sigma}} = \frac{-\gamma_4\beta_2 - \gamma_3\beta_4}{\beta_2\beta_3 - \beta_1\beta_4}, \tag{12}$$

and

$$b_{4\sigma} = \frac{-\gamma_4\beta_1 - \gamma_4\beta_3}{\beta_2\beta_3 - \beta_1\beta_4} \tag{13}$$

with $\beta_1 = (u_1 + \alpha_0 u_2)(k_+^\sigma + iZ) + p_+ u_1 + \alpha_0 q_+ u_2$, $\beta_2 = (v_1 + \alpha_0 v_2)(k_+^\sigma + iZ) - p_- v_1 - \alpha_0 q_- v_2$, $\beta_3 = (v_1 e^{-i\varphi_1} + \alpha_0 v_2 e^{-i\varphi_2})(k_-^{\overline{\sigma}} - iZ) - p_+ v_1 e^{-i\varphi_1} - \alpha_0 q_+ v_2 e^{-i\varphi_2}$, $\beta_4 = (u_1 e^{-i\varphi_1} + \alpha_0 u_2 e^{-i\varphi_2})(k_-^{\overline{\sigma}} - iZ) + p_+ u_1 e^{-i\varphi_1} + \alpha_0 q_- u_2 e^{-i\varphi_2}$, $\gamma_1 = (u_1 + \alpha_0 u_2)(-k_+^\sigma - iZ) + p_+ u_1 + \alpha_0 q_+ u_2$, $\gamma_2 = (v_1 e^{-i\varphi_1} + \alpha_0 v_2 e^{-i\varphi_2})(k_-^{\overline{\sigma}} - iZ) + p_+ v_1 e^{-i\varphi_1} + \alpha_0 q_+ v_2 e^{-i\varphi_2}$, $\gamma_3 = (v_1 + \alpha_0 v_2)(-k_+^\sigma - iZ) - p_- v_1 - \alpha_0 q_- v_2$, and $\gamma_4 = (u_1 e^{-i\varphi_1} + \alpha_0 u_2 e^{-i\varphi_2})(k_-^{\overline{\sigma}} - iZ) - p_- u_1 e^{-i\varphi_1} - \alpha_0 q_- u_2 e^{-i\varphi_2}$, where a dimensionless parameter $Z = mU/(\hbar^2 k_F)$ with $k_F = \sqrt{2m/E_F}$ is introduced to describe the barrier strength at the interface.

Calculation and results. – In fig. 2 are illustrated the spatial variations of the OP $F(x)$ in the FM/SC structure with s_{++}- and $s_\pm$-pairings for the SC, respectively, where $F(x) = (1/\pi)\sum_\sigma \int_0^\infty \mathrm{d}E\, \mathrm{Im}[G_r^\sigma(x,x,E)]_{12}$ (refs. [26,27]). As in FM/s-wave SC junctions [27], on the FM side, the proximity effect induces the superconducting OP. It is found that with increasing the distance from the interface, $F(x)$ for both the two models displays a damped oscillation and changes sign from positive (negative) to negative (positive) in the FM, *i.e.*, a transition from the "0 (π)" state to "π (0)" state, where the "0" and "π" states are, respectively, ones corresponding to the positive and negative signs of $F(x)$ [14,27,28]. Physically, the spin imbalance in the FM results in a modified Andreev process, since the incident electron and Andreev-reflected hole come from different spin subbands. As a result, the quantumn coherence in the FM between the electron near E_F and the Andreev-reflected hole can lead to spin singlet pairing correlations to have different wave vectors, so that the OP amplitude and then the local DOS in the FM both become spatially modulated, where the coherent length ξ_F in the FM is given by $\xi_F = \hbar v_F/\Gamma$. Naturally, as $\alpha_0 = 0$, the $s_\pm$ and s_{++} SCs all reduce to a conventional s-wave one, so that the results shown in fig. 2 are the same as those obtained in FM/s-wave SC junctions [27,28]. It is particularly remarkable that, with $\alpha_0 \neq 0$, the OPs on the FM and $s_\pm$-SC sides near the FM/$s_\pm$-SC interface induced by the proximity effect are not only noncontinuous but also antiphase, which is much different from those in the FM/$s_\pm$-SC and FM/s-wave SC junctions [27,28]. These differences can be explained as follows: for a single band, all incident electrons at FM/SC interface are transmitted into the same band; however, this situation is altered at $\alpha_0 \neq 0$ in a different manner for $s_\pm$- and s_{++}-pairings. For the former, all incident electrons at the FM/SC interface are transmitted into the two different bands with OPs of opposite signs; however, for the latter, although there exist two bands, they have OPs with the same signs. Consequently, the interband interference for the former different from the latter gives rise to different effects on the AR and forming a spin singlet, thus resulting in the above-mentioned different features of the OPs. The differences can be also interpreted by the fact that $e^{-i\varphi_1}$ and $e^{-i\varphi_2}$ in the expressions for the coefficients can

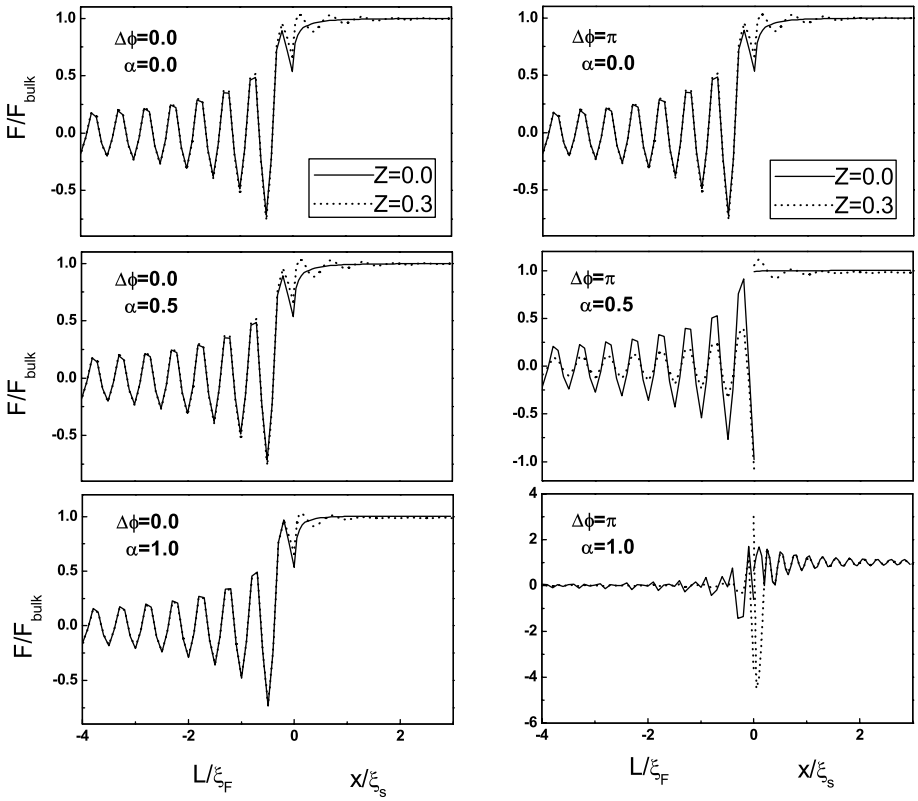

Fig. 2: Normalized spatial variation of the superconducting order parameter $F(x)$ for the s_{++} (left panels) and $s_{\pm}$ (right panels) pairing models in FM and SC with different Z, respectively. Here, $\xi_F = \hbar v_F/\Gamma$ and $\xi_S = \hbar v_F/2\Delta_1$ with $E_F = 1.4\,\mathrm{eV}$ and $\Delta_1 = 1.4\,\mathrm{meV}$, $h_0 = 15.0\,\mathrm{meV}$, $\alpha_0 = 0$, 0.5, and 1.0.

exert an important influence on the tunnelling, which are unequal for the $s_{\pm}$-pairing model and equal for the s_{++}-pairing. In addition, it is clear that the increase of Z can change $F(x)$ for both the $s_{\pm}$ and s_{++} models and the variation for the former is much bigger than that for the latter. For the s_{++} model, with increasing Z, the OP on FM side almost shows no change but has a great variation on the SC side. However, for the $s_{\pm}$ model, not only the amplitudes of the OPs on both the FM and SC sides significantly vary, but also for different α_0, the enhancement of Z has different effects on changing the sign of phase of OP at the interface. For instance, as shown in fig. 2, when $\alpha_0 = 1.0$, for $Z = 0.0$, the OP on FM and SC sides at the interface are, respectively, about -1.5 and $+0.8$, while, for $Z = 1.0$, they are about $+3.0$ and -4.0. It is also noticed that as $\alpha_0 = 0.5$, regardless of Z, the signs of the OP on FM and SC sides at the interface are not changed. These also indicate that the role of Z is strongly depedent on the interband interference in the SC. Moreover, on the SC side, the OP recovers its bulk value with the distance from the interface exceeding the coherent length ξ_S with $\xi_S = \hbar v_F/2\Delta_0$. No matter whether the case is the $s_{\pm}$- or s_{++}-paring model and no matter whether $Z = 0$ or not, this feature is not changed. Furthermore, the recalculated pair potential [26,27] $\Delta(x) = \lambda^* F(x)$, where $\lambda^* = (\lambda - \mu^*)/(1+\lambda)$ with λ the dimensionless electron-phonon coupling constant and μ^*

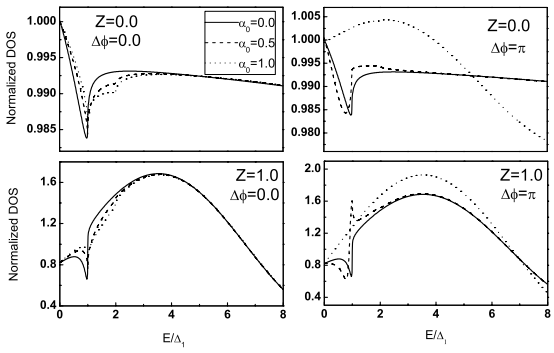

Fig. 3: Variation of electron DOS with energy for the s_{++} (left panels) and $s_{\pm}$ (right panels) pairing models in FM with the same parameters as in fig. 2 except that $x = 2.5\xi_S$.

the Coulomb pseudopotential in the SC, is equal to the bulk λ^* times $F(x \geqslant 0)$ given in fig. 2, and that in the FS is zero because $\lambda^* = 0$. This potential is not very different from the assumed one $\Delta(x) = \Delta_0\Theta(x)$, implying that the potential is now nearly self-consistent.

The local DOS of the quasiparticles is proportional to the imaginary part of the 11 components of the 2×2 retarded Green function $(x = x')$, $N(x, E) = (-1/\pi)\sum_\sigma \mathrm{Im}[G_r^\sigma(x, x, E)]_{11}$ (refs. [26,27]). In fig. 3, the DOS of quasiparticles with different Z are shown as a

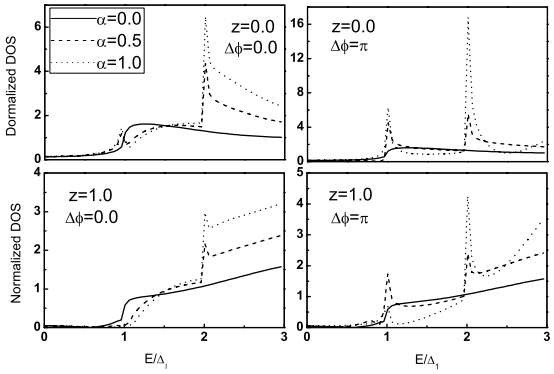

Fig. 4: Electron DOS as a function of energy for the s_{++} (left panels) and $s_{\pm}$ (right panels) pairing models in SC. The parameters are the same as those in fig. 3.

function of energy E in FM for the $s_{\pm}$ and s_{++} models, in which the DOS have been normalized by that when the SC is at its normal state. Deservedly, as $\alpha_0 = 0$, due to $s_{\pm}$ and s_{++} SCs all reducing to the same conventional s-wave one, the local DOS of both the two models are thoroughly the same no matter what the value of Z is and their behaviors with energy E for Z unequal to 0 are found similar to that of FM/s-wave SC junctions with the dip exactly at the gap energy [27,28]. With the increase of α_0, for the s_{++} model, the characteristic of the behaviors with the dip at the small gap energy is not changed whether the value of Z is equal or unequal to 0. However, for the $s_{\pm}$ model, with α_0 increased, the dip of the DOS with E is no longer at the small gap energy and shifts towards low energy until it vanishes at $E = 0$ despite the value of Z, and simultaneously, a very sharp peak of the DOS at the small gap energy also gradually appears and then disappears as $Z \neq 0$, which are much different from those for the s_{++} model. These different behaviors are just attributed to the different interband interferences in the two models. In addition, since the induced OP in the FM may give rise to the tendency of an SC-like DOS and cannot open a superconducting energy gap in FM, the induced superconductivity in the FM can be considered gapless [27].

In fig. 4, we also show the variation of the DOS of quasiparticles with energy E on the SC side for $s_{\pm}$ and s_{++} models at different α_0. It is found that owing to the proximity effect, superconductivity in the SC near the interface also becomes gapless, since the SC-like shape still remains in fig. 4, although the DOS has the biggest departure from the bulk behavior [27]. Obviously, as in figs. 2 and 3, because the $s_{\pm}$ and s_{++} SCs at $\alpha_0 = 0$ all turn into the same conventional s-wave one, the behaviors of the local DOS of both the models with energy E are just the same as those in FM/SC junctions [27] no matter what the value of Z is. With the enhancement of α_0, for both models, characteristics of the behaviors of DOS with E are not changed whether the value of Z is equal or unequal to 0. Nevertheless, the results for the $s_{\pm}$ model are much different from those for the s_{++} model. For the latter, with increasing α_0, as $Z = 0$, there exist two sharp peaks, which are, respectively, at the two gap energies, while as $Z \neq 0$, there is one sharp peak at the big gap energy. However, for the former, with increasing α_0, at any value of Z, the curve of DOS has one sharp peak at either gap energy, and the behavior at $Z = 0$ is found slightly different from that for the s_{++} model. The difference also shows that the effect of Z on the DOS of the SC side for the $s_{\pm}$ model is much greater than that for the S_{++} model, which also exactly stems from different interband interferences.

Finally, we have extended the calculation for a one-dimensional (1D) system in the previous parts, corresponding to a perpendicular incidence to replace various angles of incidence, to a three-dimensional (3D) one. After performing numerical calculations, we find that there is no qualitative difference in the calculated results between 1D and 3D approaches. Therefore, the experimental observation will provide evidence for $s_{\pm}$-pairing symmetry.

Conclusion. – In summary, we have applied the extended Nambu spinor Green's function approach to study the proximity effect in a bilayer composed of an FM and an iron-pnictide SC with antiphase s-wave pairing. It is found that on account of the opposite signs of the two pair potentials in the SC, the OPs in the FM and SC regions at the interface induced by the proximity effect are not only noncontinuous but also antiphase and the barrier strength exerts a substantial influence on the peak and dip behaviors of the induced superconducting DOS in the two regions. In particular, one conspicuously characteristic peak of the DOS is exhibited at either gap energy on the SC side. These properties are shown to be much different from those without antiphase s-wave pairing for the SC, which originates from different interband interferences of the two models. It is expected that experimental measurements of OP and DOS induced by ferromagnetic proximity effect in the present structure will confirm the antiphase s-wave pairing in iron-based SC.

* * *

This work was supported by the National Science Foundation of China under Grant Nos. 10947005, 10974170, and 110704033, the Natural Science Foundation of Jiangsu Province under Grant No. BK2009399, and the Natural Science Foundation of Jiangsu Education Department of China, under Grant No. 08KJB140004.

REFERENCES

[1] Norman M. R., *Physics*, **1** (21) 2008; Kamihara Y., Watanabe T., Hirano M. and Hosono H., *J. Am. Chem. Soc.*, **130** (2008) 3296.

[2] Chen X. H., Wu T., Wu G., Liu R. H., Chen H. and Fang D. F., *Nature (London)*, **453** (2008) 761; Wen H. H., Mu G., Fang L., Yang H. and Zhu X. Y., *EPL*, **82** (2008) 17009.

[3] Ren Z. A., Yang J., Lu W., Yi W., Che G.-C., Dong X.-L., Sun L.-L. and Zhao Z.-X., *Mater. Res. Innov.*, **12** (2008) 105; Ren Z. A., Che G.-C., Dong X.-L., Yang J., Lu W., Yi W., Shen X.-L., Li Z.-C., Sun L.-L., Zhou F. and Zhao Z.-X., *EPL*, **83** (2008) 17002.

[4] Mazin I. I., Singh D. J., Johannes M. D. and Du M. H., *Phys. Rev. Lett.*, **101** (2008) 057003; Liu R. H., Wu G., Wu T., Fang D. F., Chen H., Li S. Y., Liu K., Xie Y. L., Wang X. F., Yang R. L., Ding L., He C., Feng D. L. and Chen X. H., *Phys. Rev. Lett.*, **101** (2008) 087001.

[5] Raghu S., Qi X.-L., Liu C.-X., Scalapino D. J. and Zhang S.-C., *Phys. Rev. B.*, **77** (2008) 220503(R); Chen T. Y., Tesanovic Z., Liu R. H., Chen X. H. and Chien C. L., *Nature (London)*, **453** (2008) 1224.

[6] Drew A. J., Pratt F. L., Lancaster T., Blundell S. J., Baker P. J., Liu R. H., Wu G., Chen X. H., Watanabe I., Malik V. K., Dubroka A., Kim K. W., Rössle M. and Bernhard C., *Phys. Rev. Lett.*, **101** (2008) 097010.

[7] Stanev V., Kang J. and Tesanovic Z., *Phys. Rev. B*, **78** (2008) 184509; Shan L., Wang Y., Zhu X., Mu G., Fang L., Ren C. and Wen H.-H., *EPL*, **83** (2008) 57004.

[8] Dong J. K., Zhou S. Y., Guan T. Y., Zhang H., Dai Y. F., Qiu X., Wang X. F., He Y., Chen X. H. and Li S. Y., *Phys. Rev. Lett.*, **104** (2010) 087005; Yaagi Y., Yamakawa Y. and Ōno Y., *Phys. Rev. B*, **81** (2010) 054518.

[9] Chen W. Q., Ma F. J., Lu Z. Y. and Zhang F. C., *Phys. Rev. Lett.*, **103** (2009) 207001; Huang W. M. and Lin H. H., *Phys. Rev. B*, **81** (2010) 052504.

[10] Onari S. and Tanaka Y., *Phys. Rev. B*, **79** (2009) 174526; Bang Y., *Phys. Rev. B*, **79** (2009) 092503.

[11] Ummarino G. A., Tortello M., Daghero D. and Gonnelli R. S., *Phys. Rev. B*, **80** (2009) 172503; Ghaemi P., Wang F. and Vishwanath A., *Phys. Rev. Lett.*, **102** (2009) 157002.

[12] Ota Y., Machida M., Koyama T. and Matsumoto H., *Phys. Rev. Lett.*, **102** (2009) 237003; Ng T. K. and Avishai Y., *Phys. Rev. B*, **80** (2009) 104504.

[13] Bergeret F. S., Volkov A. F. and Efetov K. B., *Phys. Rev. Lett.*, **86** (2001) 4096; Robinson J. W. A., Witt J. D. S. and Blamire M. G., *Science*, **329** (2001) 59; Robinson J. W. A., Halász Gábor B., Buzdin A. I. and Blamire M. G., *Phys. Rev. Lett.*, **104** (2010) 207001; Kalcheim Y., Kirzhner T., Koren G. and Millo O., *Phys. Rev. B*, **83** (2011) 064510.

[14] Buzdin A. I., *Rev. Mod. Phys.*, **77** (2005) 935.

[15] Bergeret F. S., Volkov A. F. and Efetov K. B., *Rev. Mod. Phys.*, **77** (2005) 1321; Xia J., Sheluukhin V., Karpovski M., Kapitulnik A. and Palevski A., *Phys. Rev. Lett.*, **102** (2009) 087004; Sprungmann D., Westerholt K., Zabel H., Weides M. and Kohlstedt H., *Rev. Mod. Phys.*, **82** (2010) 060505; Anwar M. S., Czeschka F., Hesselberth M., Porcu M. and Aarts J., *Phys. Rev. B*, **82** (2010) 100501.

[16] Golubov A. A., Kupriyanov M. Yu. and Il'ichev E., *Rev. Mod. Phys.*, **76** (2005) 411; Oboznov V. V., Bol'ginov A., Feofanov A. K., Ryazanov V. V. and Buzdin A. I., *Phys. Rev. Lett.*, **96** (2006) 197003; Ryazanov V. V., Obozonov V. A., Rusanov A. Yu., Veretennikov A. V., Golubov A. A. and Aarts J., *Phys. Rev. Lett.*, **86** (2001) 2427; Piano S., Robinson J. W. A., Burnell G. and Blamire M. G., *Eur. Phys. J. B*, **58** (2007) 123; Robinson J. W. A., Barber Z. H. and Blamire M. G., *Appl. Phys. Lett.*, **95** (2009) 192509.

[17] Zheng Z. M., Xing D. Y., Sun G. Y. and Dong J. M., *Phys. Rev. B*, **62** (2000) 14326.

[18] Kashiwaya S. and Tanaka Y., *Rep. Prog. Phys.*, **63** (2000) 1641.

[19] Deutscher G., *Rev. Mod. Phys.*, **77** (2005) 109.

[20] Linder J. and Sudbø A., *Phys. Rev. B*, **79** (2009) 020501(R); Sperstad I. B., Linder J. and Sudbø A., *Phys. Rev. B*, **80** (2009) 144507; Linder J., Sperstad I. B. and Sudbø A., *Phys. Rev. B*, **80** (2009) 020503(R).

[21] Zhou T., Zhang D. G. and Ting C. S., *Phys. Rev. B*, **81** (2010) 052506; Tsai W. F., Yao D. X., Bernevig B. A. and Hu J. P., *Phys. Rev. B*, **80** (2009) 012511.

[22] Araújo M. A. N. and Sacramento P. D., *Phys. Rev. B*, **79** (2009) 174529; Ota Y., Machida M., Koyama T. and Matsumoto H., *Phys. Rev. B*, **81** (2010) 014502; Feng X. Y. and Ng T. K., *Phys. Rev. B*, **79** (2009) 184503.

[23] Golubov A. A., Brinkman A., Tanaka Y., Mazin I. I. and Dolgov O. V., *Phys. Rev. Lett.*, **103** (2009) 077003.

[24] de Gennes P. G., *Superconductivity of Metal and Alloys* (Benjamin, New York) 1996.

[25] Kashiwaya S. and Tanaka Y., *Rep. Prog. Phys.*, **63** (2000) 1641.

[26] McMillan W. L., *Phys. Rev.*, **175** (1968) 559.

[27] Sun G. Y., Xing D. Y., Dong J. M. and Liu M., *Phys. Rev. B*, **65** (2002) 174508.

[28] Kontos T., Aprili M., Lesueur J. and Grison X., *Phys. Rev. Lett.*, **86** (2001) 304.